Preprint Cambridge Centre for Computational Chemical Engineering ISSN 1473 – 4273

Impact of powder characteristics on a particle granulation model

Catharine A. Kastner, George P. E. Brownbridge, Sebastian Mosbach, Markus Kraft [1]

released: 1 March 2013

[1] Department of Chemical Engineering
and Biotechnology
University of Cambridge
New Museums Site
Pembroke Street
Cambridge, CB2 3RA
United Kingdom
E-mail: mk306@cam.ac.uk

Preprint No. 122

Keywords: Particle granulation, modelling, experimental characterisation, population balance equation

Edited by
Computational Modelling Group
Department of Chemical Engineering and Biotechnology
University of Cambridge
New Museums Site
Pembroke Street
Cambridge CB2 3RA
United Kingdom

Fax: + 44 (0)1223 334796
E-Mail: mk306@cam.ac.uk
World Wide Web: http://como.cheng.cam.ac.uk/

Abstract

In this paper we present a combined experimental and modelling approach to understanding the wet granulation of lactose powder in a high-shear mixer and perform a sensitivity study of the model. Experimental data is produced by performing nine granulation runs using lactose monohydrate as the initial powder and deionised water as the binder. The granulation runs were performed with variations in impeller speed, massing time and binder addition rate. The granulation process is then simulated by a population balance model published by Braumann et al. (2007) (Chemical Engineering Science, 62, 4717-4728). The model contains five rate parameters requiring estimation: coagulation, compaction, attrition, penetration and chemical reaction. The rates are estimated by sampling with Sobol sequences over a predefined parameter space. A sensitivity study reveals two important properties. First, the model input value that quantifies the height of the asperities on the particles is found to limit the model's ability to simulate even simple characterisations of the particle ensemble. However, by allowing the parameter for the height of asperities to vary over a range while estimating the rates, the simulated particle size distribution demonstrates agreement with the experimental one when using a single value characterisation. Second, the input parameters which describe the initial particle size distribution are found to significantly affect the distribution of the end product. When the input parameters which define the initial powder are allowed to vary, the model demonstrates an ability to simulate the experimental empirical size distributions.

Contents

1 Introduction

Particle granulation encompasses a vast collection of agglomeration techniques wherein a fine powder and a binder are mixed to cause the particles to grow in size. Agglomerating the particles improves flowability, dispersibility, bulk density and dusting behaviour while decreasing caking. The pharmaceuticals industry makes extensive use of granulation for these reasons, as well as to mix drugs with excipients to produce particles that are easy to dispense. Granulation is also used in the manufacture of fertilisers, detergents and is used in food processing concerns.

Granulation is performed by mixing a powder with either a liquid binder or by melt granulation. The powder is placed inside a mixer, which may be any one of a rotating drum, a fluidised bed or a high shear mixer. The binder is added to the mixing chamber and the agglomeration process commences, dependent upon the process conditions and materials employed. While on a cursory level this is a very simple process, on a kinetic level it is extremely complicated and poorly understood. Hence, the use of models and computer simulations has been incorporated into the study of granulation to further understanding of the systems while avoiding extensive experimentation. The system of interest in this paper is a high-shear wet granulation process using lactose monohydrate and deionised water. Lactose, due to its wide use as an excipient, has been used in granulation experiments to investigate many aspects of particle granulation. Studies have been performed that focus on the influence of droplet size on particle granulation [3], the influence of granulation method on compactability [49], scaling-up of granulation in high shear mixers [2], the sensitivity of the process conditions on the end product [4] and the importance of spray flux on the nucleation stage of granulation [28], among others.

Types of models used to study granulation can be loosely broken into two categories: discrete element method (DEM) and population balance models. DEM uses local contact laws to describe a finite collection of discrete bodies and is predominantly used to study flow, mixing, milling and coating processes [16, 18, 31, 43, 47]. Population balance models are based on the number balance of pre-determined classes (based on size, porosity, etc.) and use concepts of birth and death to track the evolution of a population [45]. Historically, population balance models have been single variable (size), but in the demonstrated inadequacy of such models [19, 22], various multi-variable population balance models have been proposed [9, 11, 15, 20, 22, 36, 40]. While DEM methods are capable of more detail for a given system, the associated computational expense tends to limit their use to simpler processes, short time scales and small populations. The statistical nature of population balance models make them well suited for more complicated processes with long time scales and large populations [17]. Recently, hybrid models that feed DEM results into population balance models have been constructed [17, 48]. In this paper, our attention is directed towards a multi-dimensional population balance model.

Throughout the study of granulation, a constant focus of interest has been on discerning the significant process conditions and finding how they impact the process. For example the effect of impeller speeds, binder addition rates and mixer flow patterns have been investigated, among many others process conditions [3, 5, 14, 23–26, 30, 34, 37]. While uncertainty inherent in the system is studied in the end-product of the granulation process, parameter estimates are generated exploiting this uncertainty, and attempts are made

to minimise the uncertainty in the system through experimental design, there has been very little attention paid to uncertainty in the input parameters [8, 10, 12, 13, 38, 39]. While many of these parameters can be firmly established from previous studies, uncertainty inherent in any measurement technique may be more difficult to appropriately quantify. Model input parameters that are derived from experimental measurements have uncertainty attached and, as we shall demonstrate, this uncertainty can have a significant impact on model behaviour. Further, this input error can be incorporated into the parameter estimation process to produce a more robust model and gain further understanding of the significant factors.

Although the granulation and particle technology communities have not studied this aspect of modelling, it has recently come under scrutiny in other disciplines which attempt to model complicated systems such as environmental systems, forestry processes, bacterial biofilms, seismic demand, thermal flexure microactuator responses and semiconductor wafer fabs [6, 27, 29, 33, 41, 42].

The **purpose of this paper** is to present a combined experimental and modelling approach to understanding a wet granulation process. For this purpose carefully controlled granulation experiments are performed. The data acquired is used to calibrate a detailed population balance granulation model. A model parameter study is performed to reveal sensitivities in the model which are directly related to uncertainty in the characteristics of the initial powder.

The structure of this paper is as follows: Section 2 has a description of the experimental system and powder characterisation methods. Section 3 describes the particle granulation model. Section 4 contains details of the parameter estimation process and defines the assessment criteria. In section 5 we show the results of the parameter estimation method and compare the results to the experimental data. In section 6 we draw conclusions and discuss recommendations for future work.

2 Experimental

A wet granulation process using lactose monohydrate in a bench-scale mixer is the system of interest in this study.

Experimental setup The equipment set-up that was used is shown in **Figure 1**. The experiments were performed using a horizontal axis 5 litre ploughshare mixer (Kemeutec) which is described in detail in Jones and Bridgwater [23]. The mixer shaft is driven by a variable speed DC motor with a torque meter (DRBK-20-n, ETH Messtechnik, Germany) mounted between the shaft and the motor. The mixing chamber is enclosed by a transparent plastic shield, the top of which has an aperture for a nozzle and a drip cup which is connected to a peristaltic pump (model DBP 764, Dylade Fresenius, UK).

The binder is drawn from a reservoir by a magnetic drive gear pump (model DG.19, Tuthill Corporation, USA) to a single fluid nozzle (model 121, orifice $\oslash$ 0.5 mm, 60 $^\circ$ spray angle, Düsen-Schlick, Germany) which is suspended at a fixed height above the powder bed. The pump speed is controlled by an inverter (model Altivar 31, Teleme-

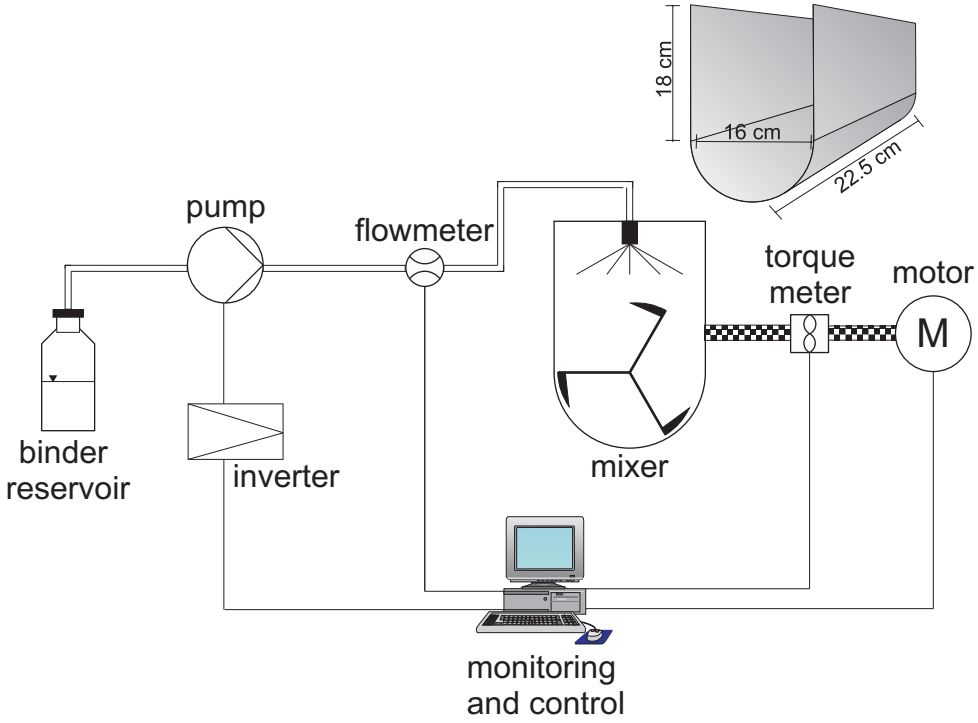

Figure 1: *Experimental setup.*

canique, France). The inverter frequency is determined by pulses from a flowmeter (OG1, Nixon Flowmeters, UK) that is mounted between the pump and the nozzle. The equipment is controlled and monitored by a Labview application that allows for the specification of binder flow rate, mixer speed, and all timing elements of the granulation process. Controlling, as well as monitoring and recording the operating status of the equipment, is facilitated by two data recording cards (6009 and 6601, National Instruments, USA).

Materials Each granulation run was performed using 1000 g of lactose monohydrate (Granulac 230, Meggle, Germany) using 150 ml deionised water as the binder. **Figure 2** shows the cumulative mass (Q_3) and the cumulative number (Q_0) distributions as well as the measured mass fractions (q_3) of the initial powder as obtained by a single 75 g sample from sieving. The cumulative mass is fitted to a lognormal distribution using the uppermost edge of each sieve class, from which the cumulative number distribution is derived using the relationship given in [1] as

$$\ln \mu_V = \ln \mu_N + 3.0 \ln^2 \sigma \,, \tag{1}$$

where μ_V and μ_N are the location parameters of a lognormal distribution for the volume and number distributions, respectively, and σ is the shape parameter.

Procedure Upon loading the mixer with the powder, the nozzle is suspended at a fixed height above the mixing chamber with the drip cup immediately below it collecting the

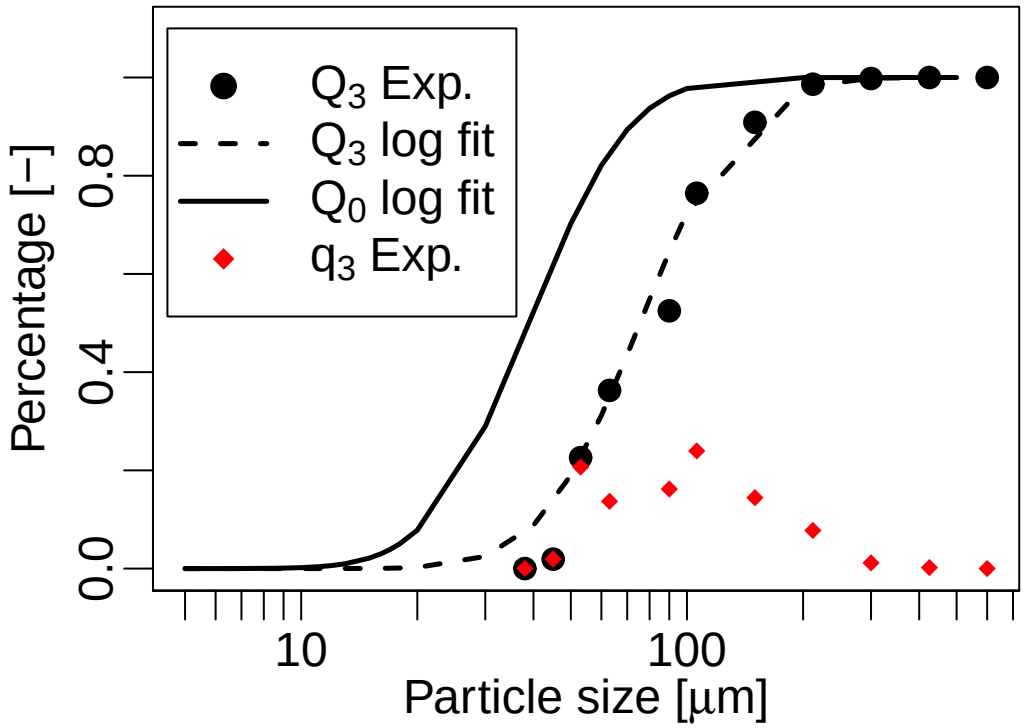

Figure 2: *Size distributions of powder used in experiments (lactose monohydrate). Normalised cumulative mass, Q_3, fit to lognormal distribution; derived number size distribution, Q_0, with lognormal fit distribution of μ_{psd} = 38.93 σ_{psd}=1.60 and fraction of mass, q_3.*

binder flow. After two minutes of dry mixing to aerate the powder, the drip cup is removed. When the allotted amount of time for the binder addition has passed, the binder stream is automatically shut off by the controller program and the drip cup is replaced under the nozzle to prevent any additional droplets from reaching the powder bed. The mixer continues to run at the specified speed until the desired amount of time has elapsed.

The resulting product is removed from the mixer and distributed onto metal trays. The trays are placed in a drying cabinet (INC 95SF, Genlab, UK) at $50\,^{\circ}$C with $55\,^{\circ}$C designated as the overheat temperature, until no significant change in mass is recorded. The dried product is recombined and samples for analysis are chosen by putting the entire dried product through a sample splitter until a sample between 50 – 90 g is obtained.

Particle size analysis is performed by sieving. Three tiers, each consisting of six sieves and a bottom pan, were constructed using a $\sqrt{2}$ progression from 53 – 16000 μm. Each tier was subjected to 25 minutes of vibration at approximately 1.5 mm amplitude on a sieve shaker (model EVL1, Endecotts, UK). Material in each of the sieves, as well as the bottom pan, was weighed and recorded giving 19 mass measurements.

Potential experimental errors A preliminary granulation run was performed in order to detect any major sources of error or sub-optimal procedures. As a result, the binder flow control was reconfigured and is measurably accurate to within $\pm$ 1 ml/min. Prior to each granulation run, the binder flow rate was tested for 150 ml of binder over the specified addition time. The granulation run was performed using control conditions that successfully produced 150 ml $\pm$ 2 ml of binder under the relevant process conditions immediately prior to each granulation run. The sieving analysis of the preliminary run allowed the selection of an appropriate range of sieves. The balances that were employed for the material and sieving measurements (XB 3200C, Precisa and 2200 P, Sartorius) are accurate to 0.01 g. The motor controller, in conjunction with the torque meter, monitors and adjusts the impeller speed at least once per second. Analysis of the recorded measurements during the granulation runs indicate that the average deviation from the specified speed for all the granulation runs is less than $\pm$ 2 rpm. **Figure 3** shows the measured speed values for an arbitrarily chosen set of experimental conditions (A4). As can be seen, while there are fluctuations, the speed does stay centred on the designated value, in this case 120 rpm, with the most extreme deviations at the beginning of the experimental run.

The process conditions were selected with a view towards having statistically detectable results with varied process conditions. Based on previously published results [4, 39, 44, 46], it was decided to fix all remaining experimental conditions, including the binder to powder ratio of 150 ml:1000 g, and to use:

1. Binder addition flow rates of 50, 75 and 100 ml/min (flow rate);
2. Mixer speed rates of 120, 180 and 240 rpm (impeller speed); and
3. Allowing the mixer to continue after all the binder had been added for 5, 10 and 15 minutes (massing time).

As a complete set of experiments would involve 3^3 granulation runs with associated particle analysis, it was decided to use a fractional factorial design of 3^{3-1}. With this choice

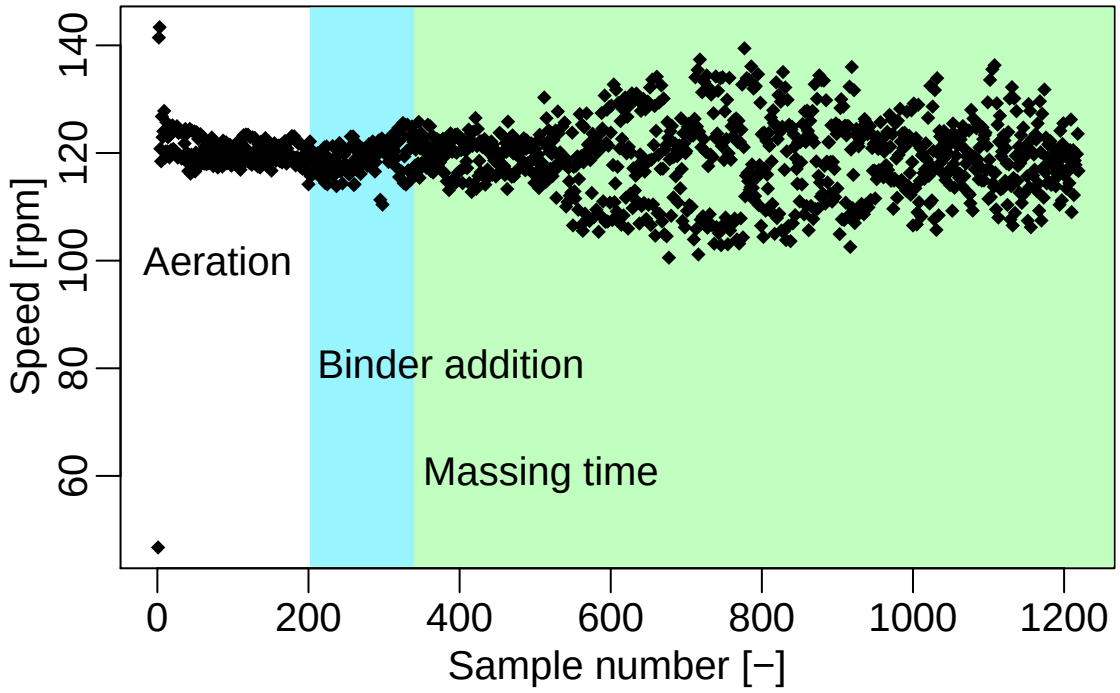

Figure 3: *Measured speed of mixer during experiment A4. White region denotes aeration stage (2 minutes). Blue region denotes liquid addition stage (90 seconds). Green region denotes massing stage (10 minutes).*

Table 1: *Selected experiments and reference codes.*

Flow rate [ml/min]	50			75			100		
Massing time [min]	5	10	15	5	10	15	5	10	15
Impeller speed [rpm]									
120			A5	B1				A7	
180	A3				A1				A8
240		A4				A2	A6		

of design, instead of performing all possible combinations of process conditions, a subset was performed which is detailed in **Table 1**, along with reference labels. See Hicks and Turner [21] for details of fractional factorial designs. The initial set of process conditions is designated by reference code B1. For case B1, 5 granulation runs were performed and five samples per run were subjected to sieving analysis. The resulting data was analysed and it was determined that three samples taken from a single granulation run would yield acceptable results. This protocol was adopted for the successive granulation runs, labelled A1 – A8. The dataset of measured mass values is included as a supplementary .csv file to this paper.

3 Model description

The granulation process is modelled using a five dimensional population balance model initially presented in 2004 at Partec [20] with the first journal publication in 2007 [9]. The individual particle volumetric properties of original solid (s_{o}), reacted solid (s_{r}), internal liquid (l_{i}), external liquid (l_{e}) and pore volume (p) are tracked as they evolve in time. The particle properties are expressed as a particle vector $x = (s_{\mathrm{o}}, s_{\mathrm{r}}, l_{\mathrm{e}}, l_{\mathrm{i}}, p)$, where each value is non-negative.

The transformations which affect the particle volume composition are liquid addition, particle coalescence, particle compaction, breakage, penetration and chemical reaction. The processes of coalescence, compaction, breakage, penetration and chemical reaction have associated rate parameters of $\widehat{k}_{\mathrm{coag}}$, $\widehat{k}_{\mathrm{comp}}$, $\widehat{k}_{\mathrm{att}}$, $\widehat{k}_{\mathrm{pen}}$ and $\widehat{k}_{\mathrm{reac}}$, respectively. A pictorial representation of the particle model and transformations is given in **Figure 4**.

Full mathematical details of the model are given in [11], and further physical reasoning about the submodels is given in [9] and [10]. Numerical details on how the stochastic particle system is used to obtain the numerical solution to the population balance equation is given in [11, 35]. Use of the model requires estimation of the five rate constants $\widehat{k}_{\mathrm{coag}}$, $\widehat{k}_{\mathrm{comp}}$, $\widehat{k}_{\mathrm{att}}$, $\widehat{k}_{\mathrm{pen}}$, and $\widehat{k}_{\mathrm{reac}}$. The input values for the model are a combination of estimated rate parameters, physical constants, and process conditions, some of which are estimated or experimentally determined. A full listing of the model input quantities and values used can be found in **Table 2**.

Table 2: *Model input values.*

Description	Symbol	Value
Known process settings		
Material density	ρ_{s_o}	1545.0 kg/m^3
Binder density	ρ_{l_e}	998.0 kg/m^3
Binder viscosity	η	1.0×10^{-3} Pa s
Impeller radius	-	72.5×10^{-3} m
Reactor volume	-	3.0×10^{-3} m^3
Impeller speed	n_{impeller}	2 – 4 rev/s
Binder flow rate	-	8.33^{-7} – 1.66^{-6} m^3/s
Wet massing time	-	300 – 900 s
Physical parameters – approximated		
Powder size distribution; location	μ_{psd}	30.0 – 45 μm
Powder size distribution; shape	σ_{psd}	1.2 – 2.8
Droplet size distribution; location	μ_{dsd}	70.0 μm
Droplet size distribution shape;	σ_{dsd}	1.0
Number of particles	-	3127540883
Solid coefficient of resistance	e_{s_o}	1.0
Reacted coefficient of resistance	e_{s_r}	1.0
Liquid coefficient of resistance	e_{l_i}	1.0
Asperities height	H_a	1×10^{-7} – 1×10^{-6} m
Physical parameters – fixed		
Relative particle velocity	U_{col}	0.1
Minimum particle porosity	-	0.25
Breakage; max size	ν_{max}	5.0
Breakage; proportion	ν_{minmax}	1.1
Breakage; minimum particle volume	-	5.236×10^{-13} m^3
Breakage; distribution	α_{daughter}	5.0
Breakage; distribution	β_{daughter}	2.0
Critical reacted solid	-	1.0×10^{20}
Rate parameters		
Coalesance rate	$\widehat{k}_{\text{coag}}$	1×10^{-14} – 1×10^{-10} m^3
Compaction rate	$\widehat{k}_{\text{comp}}$	1×10^{-15} – 1×10^{-12} s/m
Attrition rate	$\widehat{k}_{\text{att}}$	1×10^{1} – 1×10^{6} s/m^5
Penetration rate	$\widehat{k}_{\text{pen}}$	1×10^{1} – 1×10^{6} kg$^{1/2}$m$^{7/2}$/s$^{3/2}$
Chemical reaction rate	$\widehat{k}_{\text{reac}}$	5×10^{-16} – 5×10^{-9} m/s

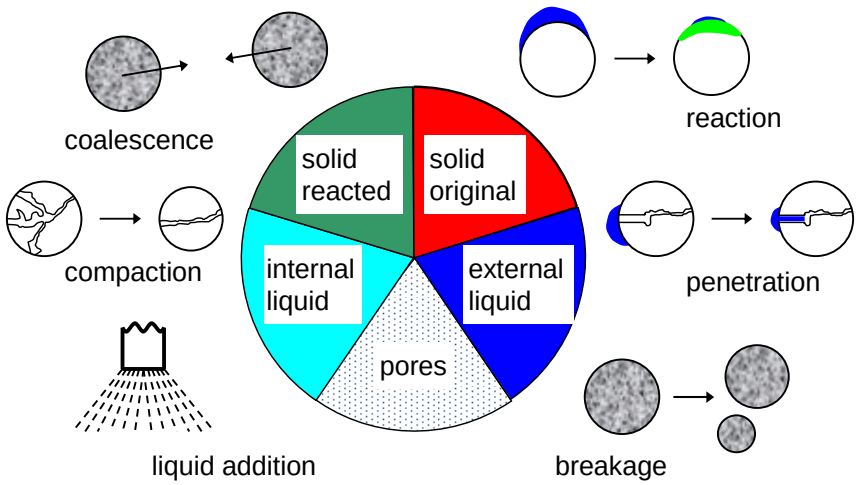

Figure 4: *Particle model and transformations in granulation process.*

3.1 Coalescence submodel

Of particular interest for our study is the model's implementation of coalescence. As described in [9] the rate parameter $\widehat{k}_{\text{coag}}$ is defined such that the collision rate of two particles x' and x'' is given by the kernel:

$$K(x', x'') = n_{\text{impeller}}\, \widehat{k}_{\text{coag}}\,, \tag{2}$$

with input parameters n_{impeller} (impeller speed) and $\widehat{k}_{\text{coag}}$ (rate constant). Thus, the number of collisions which *may* result in coalescence is controlled by the estimated rate constant and the impeller speed. However, the occurrence of successful coalescence events between two particles, once such a collision has taken place, is governed by the Stokes criterion. This is implemented under the assumption that the particle is spherical, with the particle radius given by

$$R(x) = \sqrt[3]{\frac{3}{4\,\pi}\, v(x)}\,, \tag{3}$$

where $v(x)$ is the particle volume calculated as:

$$v(x) = s_{\text{o}} + s_{\text{r}} + l_{\text{e}} + l_{\text{i}} + p. \tag{4}$$

Further, with the assumption that the densities of the liquids and the reacted solid are the same,

$$\rho_{\text{l}_\text{e}} = \rho_{\text{l}_\text{i}} = \rho_{\text{s}_\text{r}}\,, \tag{5}$$

the particle mass takes the form

$$m(x) = \rho_{\text{s}_\text{o}}\, s_{\text{o}} + \rho_{\text{l}_\text{e}}\, (s_{\text{r}} + l_{\text{i}} + l_{\text{e}})\,, \tag{6}$$

where ρ_{s_o} and ρ_{l_e} are input parameters.

The coalescence efficiency, $\widetilde{K}$, is calculated based on the Stokes criterion, which is a function of the viscous Stokes number, $\mathrm{St_v}$, and the critical Stokes number, $\mathrm{St_v^*}$, with

$$\widetilde{K}(x', x'') = \begin{cases} 1 & \text{, if} \quad e_{\mathrm{coag}}(x', x'') = 0\,, \\ 1 & \text{, if} \quad e_{\mathrm{coag}}(x', x'') > 0 \text{ and } \mathrm{St_v}^*(x', x'') \geq \mathrm{St_v}(x', x'')\,, \\ 0 & \text{, otherwise.} \end{cases}$$

The value e_{coag} is defined as the geometric average of the coefficients of restitution of the single particles x' and x'',

$$e_{\mathrm{coag}}(x', x'') = \sqrt{e(x') \cdot e(x'')} \quad . \tag{7}$$

A mass-weighted arithmetic average is used for the calculation of the coefficient of restitution of each particle,

$$e(x) = \begin{cases} \dfrac{e_{s_\mathrm{o}}\, \rho_{s_\mathrm{o}}\, s_\mathrm{o} + \rho_{l_\mathrm{e}}\, (e_{s_\mathrm{r}}\, s_\mathrm{r} + e_{l_\mathrm{i}}\, l_\mathrm{i})}{\rho_{s_\mathrm{o}}\, s_\mathrm{o} + \rho_{l_\mathrm{e}}\, (s_\mathrm{r} + l_\mathrm{i})} & \text{, if } s_\mathrm{o} + s_\mathrm{r} > 0\,, \\ 0 & \text{, otherwise (droplet),} \end{cases}$$

where $e_{s_\mathrm{o}}, e_{s_\mathrm{r}}, e_{l_\mathrm{i}} \in [0, 1]$ are input parameters. Further, we assume that $e_{s_\mathrm{o}} = e_{s_\mathrm{r}} = e_{l_\mathrm{i}}$.

The viscous Stokes number is computed as

$$\mathrm{St_v}(x', x'') = \frac{\widetilde{m}(x', x'')\, U_{\mathrm{col}}}{3\,\pi\,\eta\,\widetilde{R}(x', x'')^2}\,,$$

with input parameters U_{col} (collision velocity) and η (binder viscosity). The harmonic mass of x' and x'' is

$$\widetilde{m}(x', x'') = \frac{2\, m(x')\, m(x'')}{m(x') + m(x'')}\,.$$

The harmonic radius computes as

$$\widetilde{R}(x', x'') = \frac{2\, R(x')\, R(x'')}{R(x') + R(x'')}\,.$$

The critical Stokes number is defined by

$$\mathrm{St_v^*}(x', x'') \quad = \left(1 + \frac{1}{e_{\mathrm{coag}}(x', x'')}\right) \ln\left(\frac{h(x', x'')}{H_\mathrm{a}}\right),$$

with the input parameter H_a (characteristic length scale of surface asperities). The thickness of the binder layer $h(x', x'')$ is defined as the combined binder thickness of the particles x' and x'',

$$h(x', x'') = \frac{h(x') + h(x'')}{2}\,,$$

with the thickness of the binder layer of a particle with the properties x being calculated by

$$h(x) = \frac{1}{2}\sqrt[3]{\frac{6}{\pi}}\,\left[\sqrt[3]{v(x)} - \sqrt[3]{v(x) - l_\mathrm{e}}\right].$$

3.2 Evolution of particle ensemble

The **initial state** of the system is a set of $2^{treesize}$ particles of the form

$$x = (s_{\mathrm{o}}, 0, 0, 0, 0)$$

where $treesize$ is an integer input parameter that determines the maximum number of particles to be tracked by the model. Initially, when time is zero, all the particles in the ensemble are comprised only of original solid. The volumetric quantities of the original solid is initially populated by randomly selecting values from a lognormal distribution characterised by two input parameters, a location parameter μ_{psd} and a shape parameter σ_{psd}.

The implementation of the model is such that when a coalescence event occurs, two particles are selected from the ensemble to create a single new particle. A breakage event causes a single particle to split and its volume is randomly distributed according to a beta distribution between the two resultant entries in the particle ensemble. When the population becomes too low, less than or equal to $3/8$ of $2^{treesize}$, the population is doubled, or in other words a duplicate particle for every member of the particle ensemble is inserted into the ensemble. If the particle ensemble becomes full, a randomly selected particle is removed [11].

3.3 Post-processing

The model returns a set of particles described by the five element vector; however we need to convert the results of the simulation to a form which directly relates to our experimental results.

For each particle, x, in the final ensemble, the particle mass is calculated using Equation 5 under the assumption that, due to a drying process, all of the liquid has been removed, i.e. $l_{\mathrm{i}} = l_{\mathrm{e}} = 0$. The total volume is calculated using Equation 4. From the volume we calculate $R(x)$, the radius of the particle, using Equation 3. By doubling $R(x)$ we obtain a diameter for the particle, which can be used as a sieving diameter. All the particles in the final ensemble can then be sorted into sieve classes identical to the experimental data. The total mass in each sieve class is calculated by summing the mass for all particles sorted into a given sieve class. From these values, an empirical cumulative distribution is calculated, as with the physical system.

4 Parameter estimation methodology

In the first instance, the model has five rate parameters which need to be estimated using the experimental data. Accomplishing this requires a series of decisions with respect to the methods available and the tolerances necessary. In this implementation, one begins by defining the boundaries of the model parameter space and evaluating the model at points sampled from that space. Then one examines the set of evaluated points, seeking an optimum point or region. In this paper we make use of Sobol sequences to sample the

multi-dimensional bounded parameter space. With the sets of model evaluations, we use a variety of criteria to assess the performance of the model in comparison to the experimental results and to draw inferences from its behaviour. The 'best' Sobol point of the set is determined by some objective function; in this case specifically we use least squares, or the smallest Euclidian distance between the experimental results and the simulation, as the objective function for various methods of quantifying the results. In this section the methodology used to define the parameter space, generate the set of Sobol points and evaluate the model performance is detailed.

4.1 Parameter space

A number of factors must be considered when defining the parameter space. Theoretically, the rate parameters can range either from 0 to ∞, or from 0 to 1, but the number of collision events determined by the rates $\widehat{k}_{\mathrm{coag}}$ and $\widehat{k}_{\mathrm{att}}$ can limit the feasible ranges. The run-time of the model increases with respect to these parameters and can become prohibitively expensive when the rates become too large. A preliminary study of the run times yielded guidelines for the parameter space which will keep the run times feasible. Further, tracking a larger number of particles significantly increases the model run time. Based on the results published for this model in [11] and a preliminary convergence study, each model evaluation consists of 64 repetitions, each based on a different random number seed, and tracks 4096 individual particles. Thus, the boundaries for the rates are not only defined by the requirements of the physical system, but also by practical concerns determined by the evaluation time and model convergence.

Additionally, a smaller parameter space will yield a finer resolution for the same number of sampling points. The final parameter space used in this paper was established by an iterative process. Initially, a set of parameter boundaries was selected based on the run-time requirements and the model was evaluated over that range. The initial parameter space was deliberately chosen to be large so that it could be reduced appropriately. That space was then reduced based on a comparison of the experimental data and the results of the model. The reductions were implemented to eliminate regions which were obviously poor choices, *e.g.* when the coagulation rate was so small that particles were only being generated in the smallest five sieve classes. This process was repeated with the reduced parameter space until it was decided further reductions could possibly eliminate viable regions.

4.2 Sobol sequences

Once the parameter boundaries are fixed, a set of model evaluations is created using Sobol sequences. Sobol sequences, initially developed by I.M. Sobol in 1973, are quasi-random low-discrepancy sequences [7]. They are constructed in such a way as to generate a sequence of numbers which are both quasi-random and well-spaced as well as being computationally inexpensive. As the sequence progresses, the resolution becomes increasingly fine. To illustrate, **Figure 5** shows fifty points both randomly generated and generated from a Sobol sequence over the same region. It can be seen in the histograms that the

Sobol points fill the space more evenly. For this application, we use the Sobol points to sample the parameter space. By taking advantage of the quasi-random nature of Sobol points, we can sample from any bounded range by the simple expedient of treating it as an additional model parameter.

For each iteration in the model fitting process, 2,000 to 4,000 points were generated using a Sobol sequence. The points are mapped to the parameter space using the scheme described in [32] with a logarithmic transformation for parameters which vary over orders of magnitude and a linear transformation otherwise. The number of Sobol points was determined by the rough method of assessing the improvement, or lack thereof, in the objective functions when the number of points was doubled, beginning with 500 points. By this method a baseline of 2,000 points was established for the lower dimensional cases, which was increased to 4,000 points for the highest dimensional case. In effect this process means that for each Sobol point a parameter value is quasi-randomly selected from the parameter space. Then the model is evaluated for the 9 experimental cases at the selected set of parameter values and the objective function is calculated. The 'best' set of parameter values is designated by the smallest objective function value calculated over all of the sampled points. To give a sense of the model runtimes required, one of the final 2000 Sobol point runs required 32 CPUs (in parallel) approximately 12 hours to complete 18000 individual model evaluations.

4.3 Additional parameters of interest

While the model requires estimation of the five rate parameters, it is initially assumed that the remaining physical parameters are fixed values. However, while attempting to simulate the experimental data, the model demonstrated sensitivity to two aspects of the powder characterisation.

4.3.1 Height of asperities

Regardless of how we choose to quantify the height of asperities for a given powder, any single value characterisation will perforce be an approximation, as different particles will have asperities of varying heights. For this powder, as we have no experimental data to inform our decisions, we begin with an initial estimate of 1.0μm for the height of asperities. However, as any single value is an approximation which would need to be adjusted until it achieved some abstract state of correctness, we propose instead to define a range based on 'reasonable' physical boundaries which will be refined by the behaviour of the model. The performance of the model with respect to particle size growth suggests that 1.0 μm belongs at the upper bound of the range, thus we choose to explore a range of 0.1–1.0 μm.

Further, by nature of the Sobol sequences, we can easily sample from this range by treating it as a sixth parameter. The model continues to use a single value characterisation for the height of asperities for each set of rates; however that value is quasi-randomly selected from the range. With the addition of a sixth parameter, 2,000 Sobol points were found to be adequate to sample the parameter space.

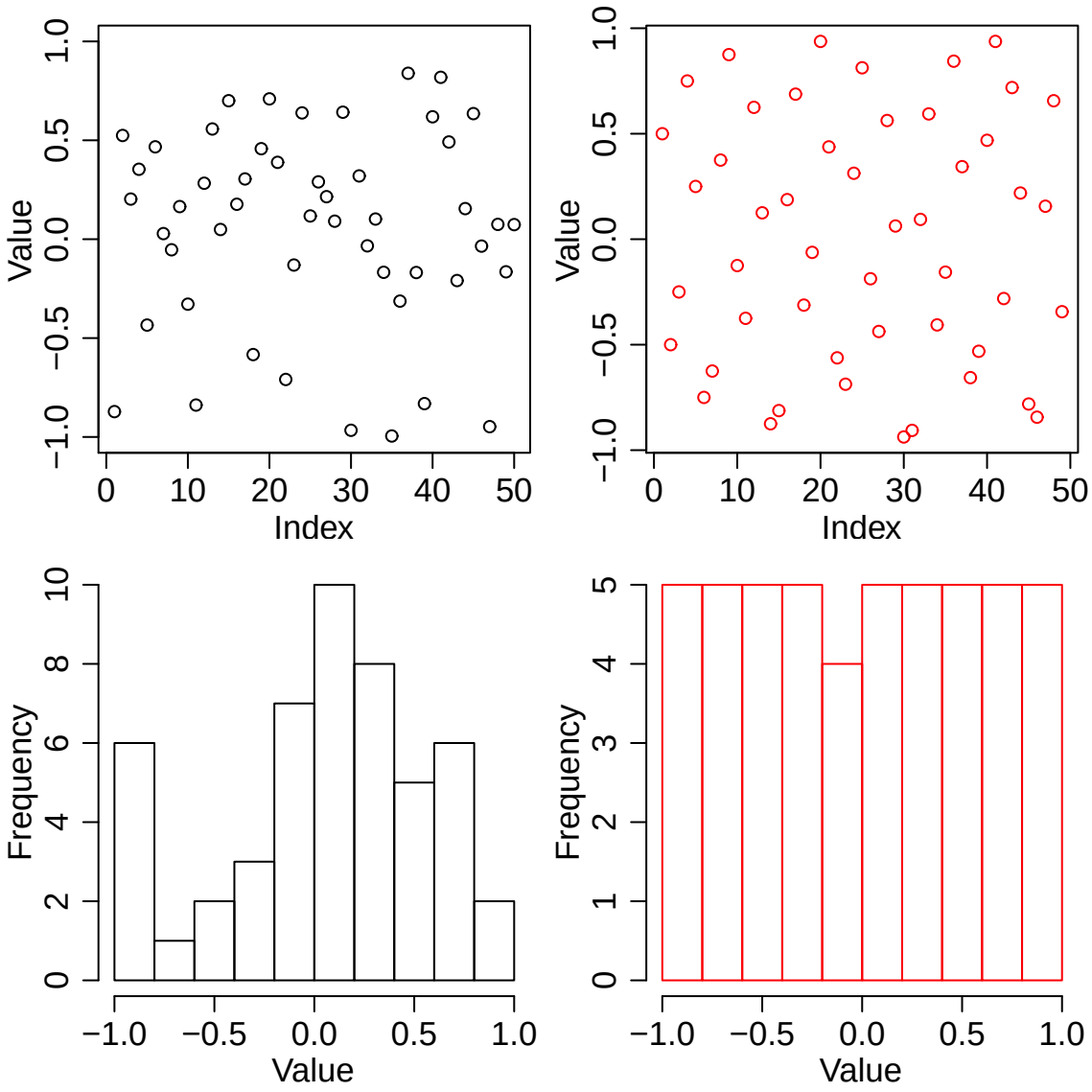

Figure 5: *Comparison between 50 uniformly distributed points (black) and 50 Sobol sequence points (red).*

4.3.2 Initial powder size distribution

The initial powder size distribution is based on experimental data as discussed in Section 2. The model inputs are $\mu_{\text{psd}} = \exp(\mu_N)$ and $\sigma_{\text{psd}} = \exp(\sigma)$ where μ_N and σ define a lognormal curve based on the estimated number distribution of powder sieving data. However, μ_N and σ are derived from experimental measurements and contain uncertainty, both from the measurement technique and the curve-fitting process. Given this uncertainty, we construct ranges around the experimentally determined input values and sample from those ranges with Sobol points in the same manner used with the height of asperities. By beginning with large ranges for both parameters based around the initial estimates and reducing them to viable regions, we have final ranges of 20 – 45 μm for μ_{psd} and 1.2 – 2.0 for σ_{psd} with the sieving based estimates of 38.93 and 1.60, respectively. This is equivalent to 2.99 – 3.80 for μ_N and 0.182 – 0.693 for σ with sieving data estimates of 3.66 and 0.47, respectively. With the inclusion of these two additional parameters, we generate 4,000 Sobol points in an eight-dimensional space.

4.4 Criteria for objective function

In the experimental portion of the work, we obtain a vector of sieving measurements which describe the end-product of the particle size distribution. There are many ways to express these results quantitatively and we shall use more than one to assess the performance of the model. In all cases, as the considered quantities are similar in order of magnitude, we shall use the Euclidian distance as the objective function. To accomplish this, we select an observable quantity f, *e.g.* the empirical geometric mean particle size, and then for each model evaluation we calculate a value:

$$OF = \sqrt{\sum_{j=1}^{N}\sum_{i=1}^{M}(f_{ij}^{\text{sim}} - f_{ij}^{\text{exp}})^2}\,, \tag{8}$$

where N is the number of experimental runs and M is the number of responses for each criterion, f^{sim} is the response from the simulation and f^{exp} is the response from the experimental data. In this manner we obtain a numeric expression of the fit of the model to the experimental data. The single variate functions that we will use for $f(x)$ are the empirical geometric mean particle size and the empirical variance. Further, we shall use the multivariate characterisations of categorical quantiles and empirical cumulative distribution. For all of these functions, the best parameter set is considered to be the set with the smallest objective function value.

4.4.1 Empirical cumulative distribution

The values for this objective function are determined directly from the experiments and the post-processing of the model. The vectors are derived from mass fractions that are expressed as a N dimensional vector d, where N is the number of sieve classes. The

density can also be physically interpreted as the percentage of mass that is found in each sieve class. These values are calculated as:

$$d_i = \frac{m_i}{\sum_{j=1}^{N} m_j} \,, \tag{9}$$

where m_i is the mass measured in the ith sieve class by sieving or postprocessing.

From this point, we convert the values into an empirical cumulative distribution function by summing all fractions of mass that are smaller than a given sieve class. This is equivalent to sieving measurements in terms of proportions of material that have passed through any given sieve aperture. The empirical distribution function, D, is also a N dimensional vector, which is calculated directly from the mass fractions as:

$$D_i = \sum_{j=1}^{i} d_j \,, \tag{10}$$

where $i = 1, \ldots, N$.

4.4.2 Empirical geometric mean particle size

The empirical geometric mean particle size, M_g, is a single value expression used to describe the particle size distribution. In this context, we use the geometric mean particle size, wherein we transform the sieve aperture values, x, by taking the natural log. This transformation is used so that the larger particle size classes are not disproportionately represented. In the sieve series that we use, the range of the sieve classes is 53 μm – 16000 μm which, by taking the natural log, transforms into 3.97 – 9.68, i.e. $x' = \ln(x)$. The empirical geometric mean particle size is calculated by first multiplying the density by the transformed sieve class and then taking the exponential of the summed the results:

$$M_g = \exp\left(\sum_{i=1}^{N} d_i x_i'\right) \,, \tag{11}$$

where each d_i is the ith element of the N dimensional density function and x_i' is the upper bound of the ith sieve class under the natural log transformation.

4.4.3 Empirical variance

The variance, Var is a single value expression of the spread of the resultant particle size distribution. For this value, we shall use the untransformed sieve class values, i.e. using the arithmetic means. The variance is calculated as:

$$Var = \sum_{i=1}^{N} d_i x_i^2 - \left(\sum_{i=1}^{N} d_i x_i\right)^2 \tag{12}$$

where each d_i is the ith element of the N-dimensional density function and x_i is the upper bound of the ith sieve class.

4.4.4 Categorical percentile

In powder studies, one of the more popular methods of describing the materials is by using percentiles, specifically the 10th, 50th and 90th percentiles. However, to analyse our data using these values some choices need to be made, as we are using categorical data. One way to quantify a percentile value is based on the category, or sieve class. If one uses an index as the category identifier, then one can find the category where the desired quantile belongs. For example: if the ECDF is: 0.0077, 0.028, 0.083, 0.2155, 0.3993, 0.5953, 0.7683, 0.8947, 0.9778, 0.9915, 1.0; then the 10th percentile is in the 3rd sieve class, the 50th percentile is in the 5th sieve class and the 90th is in the 8th sieve class. This process gives a vector which expresses how far away from the experimental sieve classes the model results are. In addition to the usual objective function, we can also sum the three numbers to get a deviation score for all three measurements. For example if the experimental data has [3, 6, 9] as the 10th, 50th and 90th percentiles, respectively, and the model produces [2, 4, 11]; the differences are [1, 2, 2], which gives 5 for that set of experimental conditions.

5 Results

5.1 Model results

The final, iteratively determined, parameter space is detailed below in **Table 3**. We perform runs of 2,000 to 4,000 Sobol points on this space with the model under three different situations. The selection of the three parameter sets is based on sensitivities observed during preliminary model evaluations. The first model configuration uses 2,000 Sobol points for the five rate parameters with fixed values for the height of asperities and for the two parameters, μ_{psd} and σ_{psd}, that determine the initial powder size distribution. The second also uses 2,000 Sobol points and incorporates the height of asperities, H_{a}, as a sixth parameter while maintaining fixed values for μ_{psd} and σ_{psd}. The third situation uses 4,000 Sobol points for eight parameters, μ_{psd} and σ_{psd} in addition to the five rate parameters and H_{a}. The ranges for the μ_{psd}, σ_{psd} and H_{a} are expansions upon the five-parameter setup based on the models behaviour with respect to the fixed values of 38.93μm, 1.60 and 1×10^{-6}m. In the following discussion, the focus will be upon the behaviour of these parameters and the rate parameter for $\widehat{k}_{\mathrm{coag}}$, as these parameters were observed exhibit the most influence on the results.

5.2 Experimental results

The mass fraction vector, q_3, is obtained directly from laboratory measurements. The empirical cumulative distribution, Q_3, is then calculated by Equation 10 for each sample,

Table 3: *Parameter space used in simulations.*

Parameter	Lower bound		Upper bound	Scaling
$\widehat{k}_{\mathrm{coag}}$	1×10^{-14}	–	1×10^{-10}	logarithmic
$\widehat{k}_{\mathrm{comp}}$	1×10^{-15}	–	1×10^{-12}	logarithmic
$\widehat{k}_{\mathrm{att}}$	1×10^{1}	–	1×10^{6}	logarithmic
$\widehat{k}_{\mathrm{pen}}$	1×10^{1}	–	1×10^{6}	logarithmic
$\widehat{k}_{\mathrm{reac}}$	5×10^{-16}	–	5×10^{-9}	logarithmic
H_{a}	1×10^{-7}	–	1×10^{-6}	logarithmic
μ_{psd}	20μm	–	45μm	linear
σ_{psd}	1.2	–	2.0	linear

where q_3 is the equivalent of d. For each set of process conditions, an averaged Q_3 is calculated for each sieve class over all samples. All of the experimental results given are calculated by using the averaged Q_3 directly or the averaged q_3 values derived from the averaged Q_3.

MANOVA analysis of the resulting mass distributions indicates that differences in the found distributions are statistically significant. Further, the calculated geometric mean particle size, as calculated from the distributions, appears to converge over time. This suggests that a process condition independent end-point may have been found for this experimental system, within the boundaries of the process conditions.

5.3 Empirical geometric mean particle size criterion

The smallest objective function values and their rates as determined by the optimisation process based on the calculated empirical geometric mean particle size can be seen in **Table 4**. It can clearly be seen that the model's ability to simulate the empirical geometric mean particle size is significantly affected by the number of parameters in the model configuration, as the objective function is more than halved when the additional parameters are introduced. In addition, in **Figure 6** we can see how well the model performs under individual process conditions. The five-parameter case either over- or underestimates the empirical geometric mean particle size in all cases and the discrepancy is often more than 200 μm. However, with the exception of the B1 experimental case, the six- and eight-parameter cases predict the values with more accuracy and follow the trends observed in the experimental quantities. The six- and eight-parameter cases demonstrate an equivalent ability to predict the results which the five-parameter case clearly does not possess, however it is interesting to note that while the six-parameter case has a smaller objective function value, the eight-parameter case appears to observe the trends evident in the experimental data more accurately. It should be noted that the rates selected for $\widehat{k}_{\mathrm{coag}}$ are of similar magnitude for all three cases, while the μ_{psd} and σ_{psd} parameters in the eight-parameter case shift a relatively small degree from the fixed values. The selected

Table 4: *Objective function and best estimated parameters where empirical geometric mean particle size is selection criterion.* **Fixed parameters are in bold**.

	5 parameters	6 parameters	8 parameters
Objective function	1079.35	362.54	372.01
$\widehat{k}_{\text{coag}}$	2.90×10^{-13}	1.72×10^{-13}	2.13×10^{-13}
$\widehat{k}_{\text{comp}}$	1.01×10^{-13}	2.14×10^{-14}	2.89×10^{-13}
$\widehat{k}_{\text{att}}$	24335	1833	236
$\widehat{k}_{\text{pen}}$	27	994394	871336
$\widehat{k}_{\text{reac}}$	1.08×10^{-14}	1.37×10^{-11}	7.83×10^{-10}
H_{a}	$\mathbf{1 \times 10^{-6}}$	2.52×10^{-7}	3.40×10^{-7}
μ_{psd}	$\mathbf{38.93 \mu}$m	$\mathbf{38.93 \mu}$m	31.7μm
σ_{psd}	**1.60**	**1.60**	1.62

μ_{psd} has a slight downward shift and σ_{psd} increases slightly. The selected H_{a} parameter however, has a significant and similar decrease from the five-parameter fixed value for both alternate cases. This suggests that the H_{a} is significant with respect to this form of describing the particle size distribution and our initial guess of 1.0 μm is too large.

5.4 Empirical variance criterion

The smallest objective functions and rates that were selected by optimising the variance of the resulting particle size distribution can be seen in **Table 5**. Interestingly, while all the objective functions are of a similar order of magnitude, the five-parameter case is marginally smaller than the others and the six parameter case is slightly smaller than the eight parameter case. Further, in **Figure 7** we can see that all cases are largely equal in performance, with the A2 experimental case being the exception to the model following the experimental trends. The rates selected by the objective functions should be noted, insofar that the chosen $\widehat{k}_{\text{coag}}$ parameters are two orders of magnitude larger than for the geometric mean particle size. This can be understood as a result of the method by which the variance is calculated such that large particle sizes will have more influence. This suggests that in order to optimise the variance all selected cases generate larger particles then when optimising the empirical geometric mean particle size. Further, note that again the six- and eight-parameter selection for H_{a} is similar and larger than for the geometric mean particle size. Interestingly, taken together with the rates, this indicates that more coagulation events are happening, with a lower success rate than with the geometric mean particle size. Additionally, we see a further downward shift in the value for μ_{psd} and a further increase in σ_{psd}. This indicates that the selected initial distribution is centred at a lower value, but is more widely spread than with the fixed conditions, a by-product of which is that the initial powder would have a larger variance than with the fixed values.

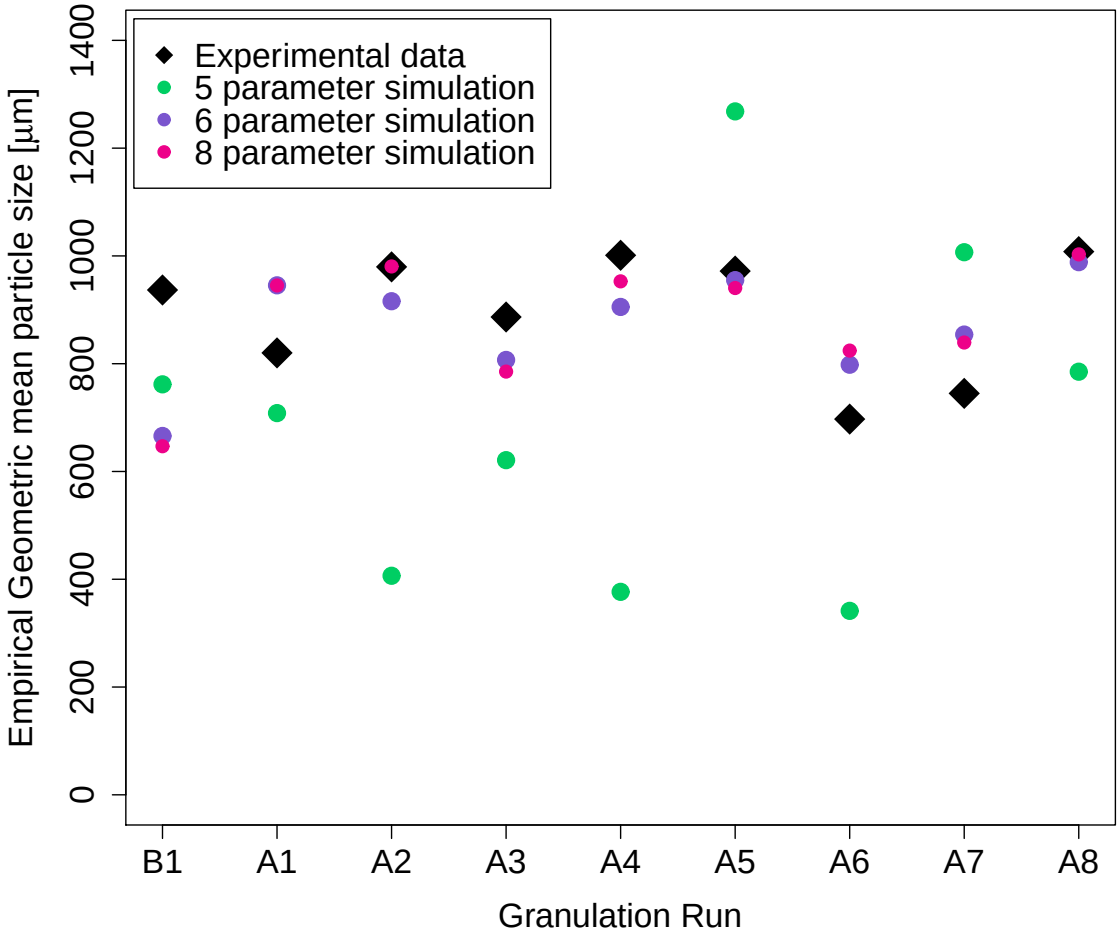

Figure 6: *Experimental results with best set of simulations. Empirical geometric mean particle size is optimisation criterion.*

Table 5: *Objective function and best estimated parameters where empirical variance is selection criterion.* **Fixed parameters are in bold**.

	5 parameters	6 parameters	8 parameters
Objective function	11541339	12675168	13959977
$\widehat{k}_{\text{coag}}$	3.44×10^{-11}	5.44×10^{-11}	9.59×10^{-11}
$\widehat{k}_{\text{comp}}$	3.13×10^{-15}	9.04×10^{-15}	4.76×10^{-14}
$\widehat{k}_{\text{att}}$	1895	24	980
$\widehat{k}_{\text{pen}}$	965	13260	24853
$\widehat{k}_{\text{reac}}$	7.58×10^{-16}	1.83×10^{-12}	9.10×10^{-14}
H_{a}	$\mathbf{1 \times 10^{-6}}$	5.99×10^{-7}	5.60×10^{-7}
μ_{psd}	$\mathbf{38.93 \mu}$m	$\mathbf{38.93 \mu}$m	29.7μm
σ_{psd}	**1.60**	**1.60**	1.84

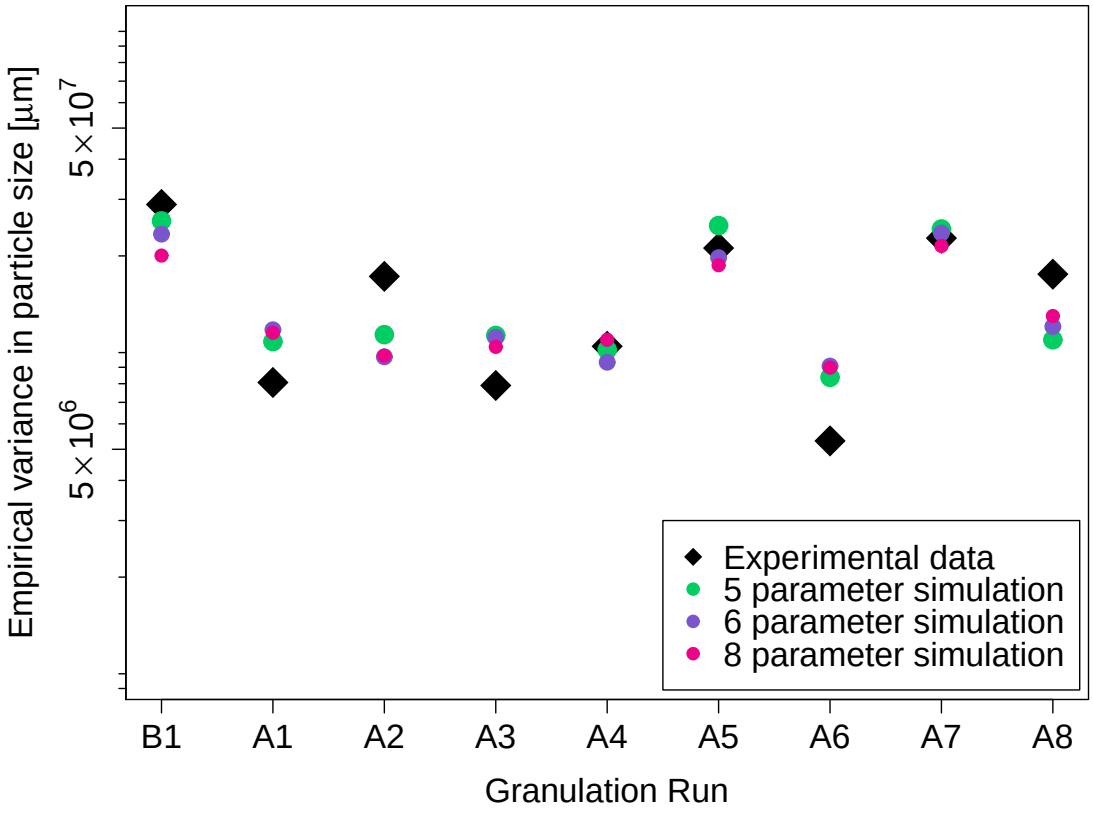

Figure 7: *Experimental results with best set of simulations. Empirical variance is optimisation criterion.*

5.5 Categorical percentile size criterion

The results of the objective function and the rates that were selected by the optimisation process based on the 10th, 50th and 90th percentiles, when treated as strictly categorical data, can be seen in **Table 6**. Additionally, the absolute distance between the simulated sieve classes and the experimental points is included. The objective function decreases slightly with the addition of the sixth parameter and is decreased by $1/3$ for the eight-parameter case when compared to the five-parameter case. In **Figure 8** we can again see that for all experimental cases, the five-parameter system is consistently over- or undersized. We can observe a slight improvement overall with the six-parameter case, but in most experimental cases the behaviour for the five- and six-parameters cases is similar. Additionally, by the counts portrayed by the objective function values and in the figures, one can see that while the eight-parameter case may deviate one, two, or, on three occasions, 3 sieve classes from the experimental results, the five and six-parameter configurations deviate by 3 sieve classes at least five times and by 4-5 sieve classes multiple times. Further, note that while the 10th percentile is exactly matched by all parameter configurations for three sets of process conditions, the 90th percentile is only simulated exactly in one instance by the 8 parameter case. While the eight-parameter case deviates by one or two sieve classes from the 90th percentile class, the five- and six-parameter cases frequently deviate by 3 or more classes.

With respect to the selected rates, while the selection for $\widehat{k}_{\mathrm{coag}}$ has returned the area selected by the geometric mean particle size method for the five- and six- parameter configurations, the eight-parameter case has remained in the area that was selected by the variance-based optimisation. This suggests that the parameter values selected for the variance were created an oversized particle size distribution, with respect to the geometric mean particle size, for the five- and six-parameter cases. Further, this suggests that the values selected for the geometric mean particle size are not representative of an accurate variance in all cases. The value for H_{a} is again increased to a similar degree for the six- and eight-parameter cases, to the point that it only deviates marginally from the fixed value for the five-parameter case. Further, we again note that for the eight parameter case there is a noticeable increase in the σ_{psd} with a minor decrease in the μ_{psd}. Overall, this suggests that that the shape of the distribution is more significant than its location when attempting to simulate more complicated assessments of the experimental data.

5.6 Empirical cumulative size distribution criterion

Next, we use a more detailed form of model output. Here, we shall examine the empirical cumulative size distribution (ECDF) for all of the experimentally measured values. The objective function and selected rates are displayed in **Table 7**, where the same pattern of decreasing objective functions is shown for the model configurations. In **Figure 9** we can directly compare how the selected simulated ECDF fits the experimental data. Here we can see that the shape of the resultant ECDF remains largely the same for the five- and six-parameter scenarios, and in neither case are they a particularly good fit to the experimental results. The five- and six- parameter cases consistently fail to produce particles in the larger sieve classes and also show a tendency to place an inappropriate amount

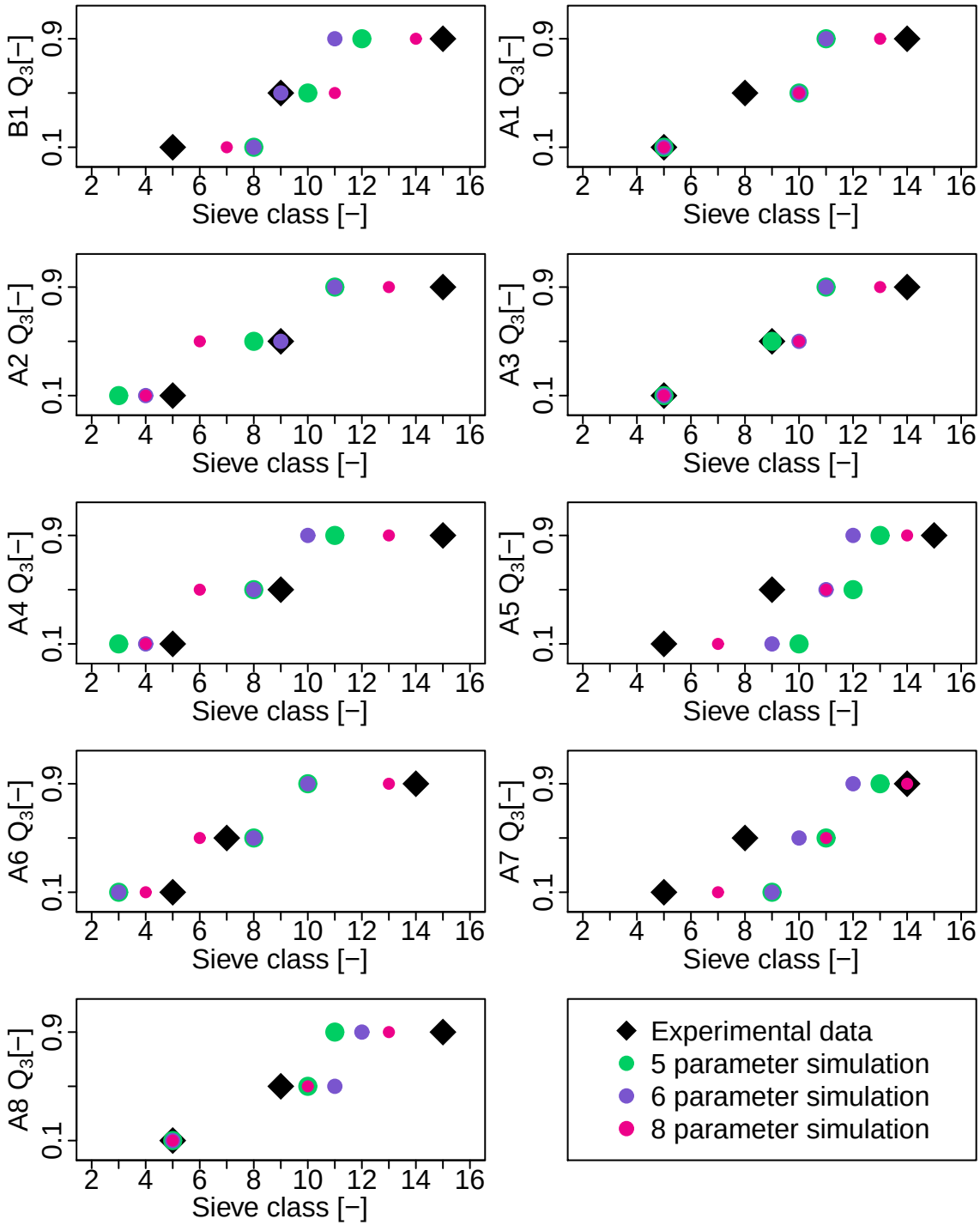

Figure 8: *Experimental results with best set of simulations. 10th, 50th and 90th percentiles are optimisation criterion.*

Table 6: *Objective function and best estimated parameters where categorical sieve class for 10th, 50th and 90th percentile is selection criterion.* **Fixed parameters are in bold**.

	5 parameters	6 parameters	8 parameters
Objective function	13.60	13.37	8.60
Absolute distance	59	57	38
$\widehat{k}_{\text{coag}}$	7.84×10^{-13}	3.95×10^{-13}	2.07×10^{-11}
$\widehat{k}_{\text{comp}}$	2.92×10^{-15}	2.13×10^{-13}	6.96×10^{-14}
$\widehat{k}_{\text{att}}$	3659	993	12051
$\widehat{k}_{\text{pen}}$	55	23	1592
$\widehat{k}_{\text{reac}}$	7.51×10^{-12}	4.41×10^{-13}	1.15×10^{-15}
H_{a}	$\mathbf{1 \times 10^{-6}}$	8.56×10^{-7}	9.66×10^{-7}
μ_{psd}	$\mathbf{38.93\mu}$m	$\mathbf{38.93\mu}$m	35.6μm
σ_{psd}	**1.60**	**1.60**	1.90

of the mass in a few, closely spaced, size classes. The eight-parameter case, however, demonstrates the ability to alter the constructed curve to create a better fit. Although none of the configurations show an ideal fit to the ECDF, the eight-parameter case appears to have the capacity to fit the experimental results, while the others are far less promising. One aspect of the illustrations to note is that in the experimental results, the large sieve classes would have a relatively small population of particles, often one or two particles in the largest classes, which, given the nature of the population balance model, would be difficult to capture without tracking an inordinate number of particles. Nevertheless, the model seems to demonstrate that with the more complicated form of the results, the inclusion of H_{a} as well as the μ_{psd} and σ_{psd} as parameters enables the model to simulate the experimental results.

The selected rates demonstrate the same pattern as with the categorical sieve classes insofar that μ_{psd} shows a slight decrease and σ_{psd} shows a marked increase. The selected values for H_{a} are similar across the six- and eight-parameter cases and the rates overall are of similar magnitude to the categorical sieve class assessment.

5.7 Overall analysis of powder characterisation

Lastly, we examine the feasibility of the proposed H_{a}, μ_{psd} and σ_{psd} which the objective functions have selected. Of all the rate parameters and experimental parameters, this is the only aspect where we can assess if the values that are being selected are realistic. With respect to the H_{a}, the model is suggesting that the powder has smaller asperities than the initial approximation. The validity of this suggestion can only be established through future experimentation.

The initial powder distribution however, does have sieving data to form a basis for com-

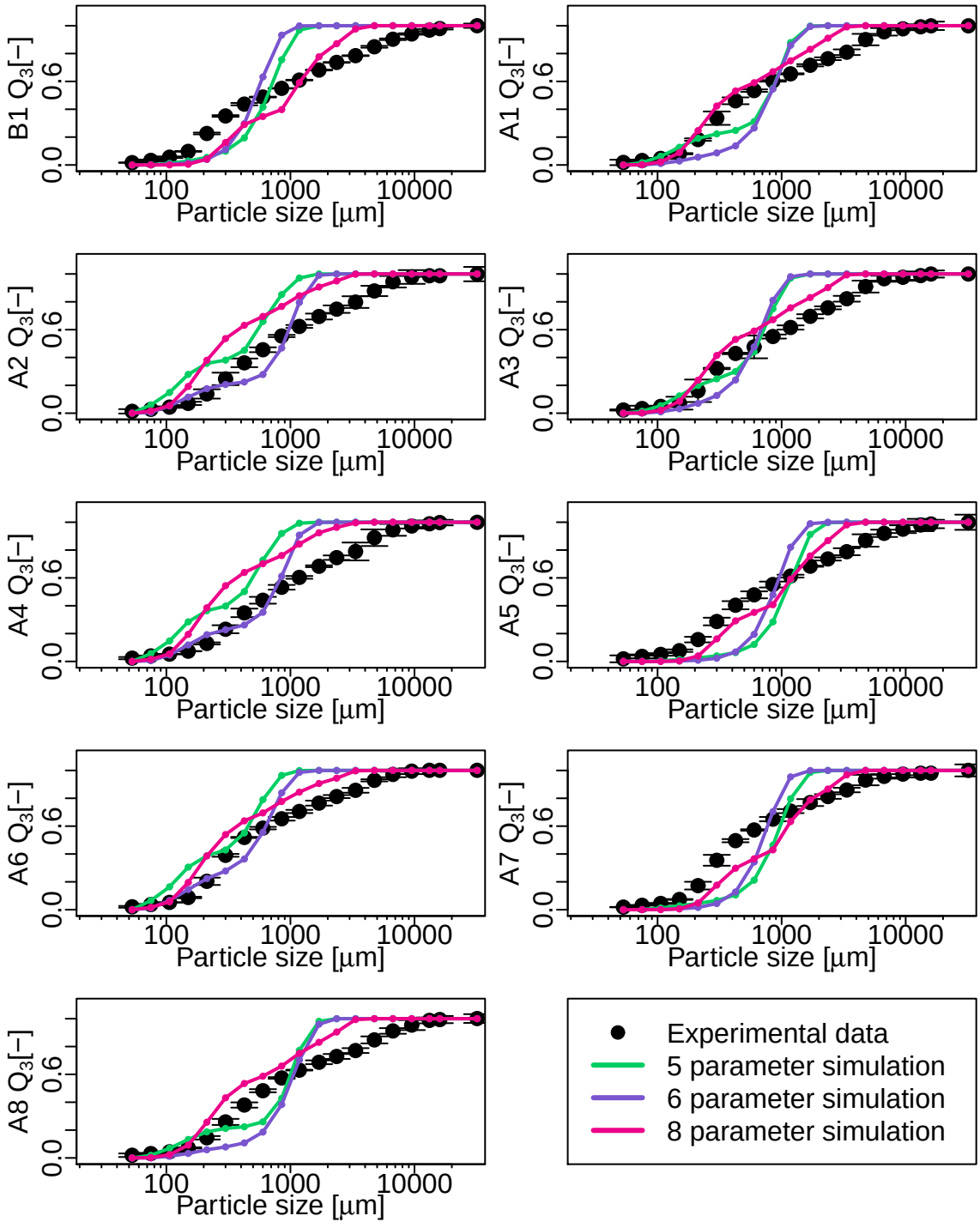

Figure 9: *Experimental results with best set of simulations. Empirical cumulative distribution function is optimisation criterion.*

Table 7: *Objective function and best estimated parameters where empirical cumulative distribution function is selection criterion.* **Fixed parameters are in bold**.

	5 parameters	6 parameters	8 parameters
Objective function	2.16	2.03	1.58
$\widehat{k}_{\text{coag}}$	2.52×10^{-13}	1.42×10^{-13}	3.03×10^{-11}
$\widehat{k}_{\text{comp}}$	1.21×10^{-15}	1.07×10^{-14}	9.35×10^{-15}
$\widehat{k}_{\text{att}}$	5364	658	271
$\widehat{k}_{\text{pen}}$	38	28	6530
$\widehat{k}_{\text{reac}}$	2.14×10^{-13}	6.19×10^{-13}	9.22×10^{-14}
H_{a}	$\mathbf{1 \times 10^{-6}}$	6.11×10^{-7}	8.66×10^{-7}
μ_{psd}	$\mathbf{38.93\mu}$m	$\mathbf{38.93\mu}$m	37.9μm
σ_{psd}	**1.60**	**1.60**	1.97

parison. In **Figure 10** and **Figure 11** we can see the model suggested fit lines plotted against the experimental mass measurements and the derived lognormal fit lines for the number and mass distributions of the initial powder. In all instances, the values selected for μ_{psd} were of smaller than the fixed value and found values for σ_{psd} were noticeably larger. Bearing in mind that the model input values are the number distribution, we can observe the rightward shift and increased spread of the selected distributions. None of the alternative combinations of μ_{psd} and σ_{psd} appear to be unreasonable with respect to the number distribution, particularly when one considers the mechanical nature of sieving analysis.

When the selected number distributions are converted into mass distributions, the proposed changes become more evident and less credible. With respect to mass, the selected distributions range from moderately undersized to markedly larger then the measured values. If one interprets the tendency to select significantly larger values for σ_{psd} and smaller values for μ_{psd} to indicate that the shape of the distribution is more significant, a value of μ_{psd} could be selected to remedy this disparity, akin to the values found for the variance. Further, the method of sieving analysis forces us to make a choice as to how to define the particle size with respect to the data points. In this paper, we have used the uppermost point of the sieves for the curve fitting, but using the midpoint or the lower most edge of the sieve classes are choices which could also be justified. Either of these choices would generate a smaller value for μ_{psd}, while maintaining the value for σ_{psd}. However, as the bounds for the model were arbitrarily established, it would be inappropriate to make any concrete statement with respect to the powder distribution without experimental verification.

With these observations, a number of possibilities should be considered. Firstly, there may be a kinetic mechanism which the model does not possess that causes the disparity. Alternately, if the model does possess the relevant mechanisms, then characterisation of the powder by either the sieving data or the lognormal curve is insufficient for the model.

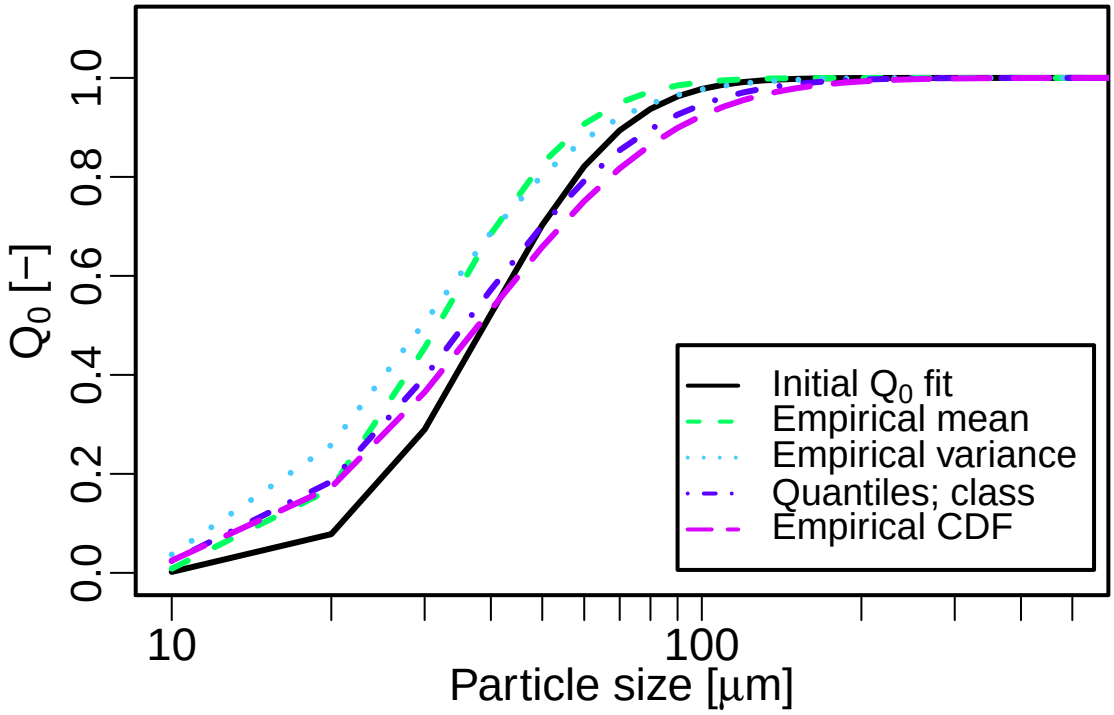

Figure 10: *Initial powder number distribution found by various objective functions.*

In either case, the suggestion that the shape of the distribution is significantly affecting the end-product should be investigated. A further complication that should be noted is the difference, sometimes by orders of magnitude, in the optimal rates selected by the various objective functions. While this disparity could result from local minima being found in a non-smooth parameter space, it should be the subject of further study.

6 Conclusions

We have presented a combined experimental and modelling approach to understanding the wet granulation of lactose powder in a high-shear mixer. Experimental data produced by performing nine wet granulation runs using lactose monohydrate as the initial powder and deionised water as the binder is presented and included as a supplementary .csv file. The granulation runs were performed with variations in impeller speed, massing time and binder addition rate and then simulated by a population balance model containing five rate parameters requiring estimation. The rates are estimated by sampling with Sobol sequences over a pre-defined parameter space.

The methodology used to perform the parameter estimation is found to yield useful results. By using Sobol sequences as a means to sample the parameter space, we are able to create a map of the parameter space and assess the behaviour of the parameters with

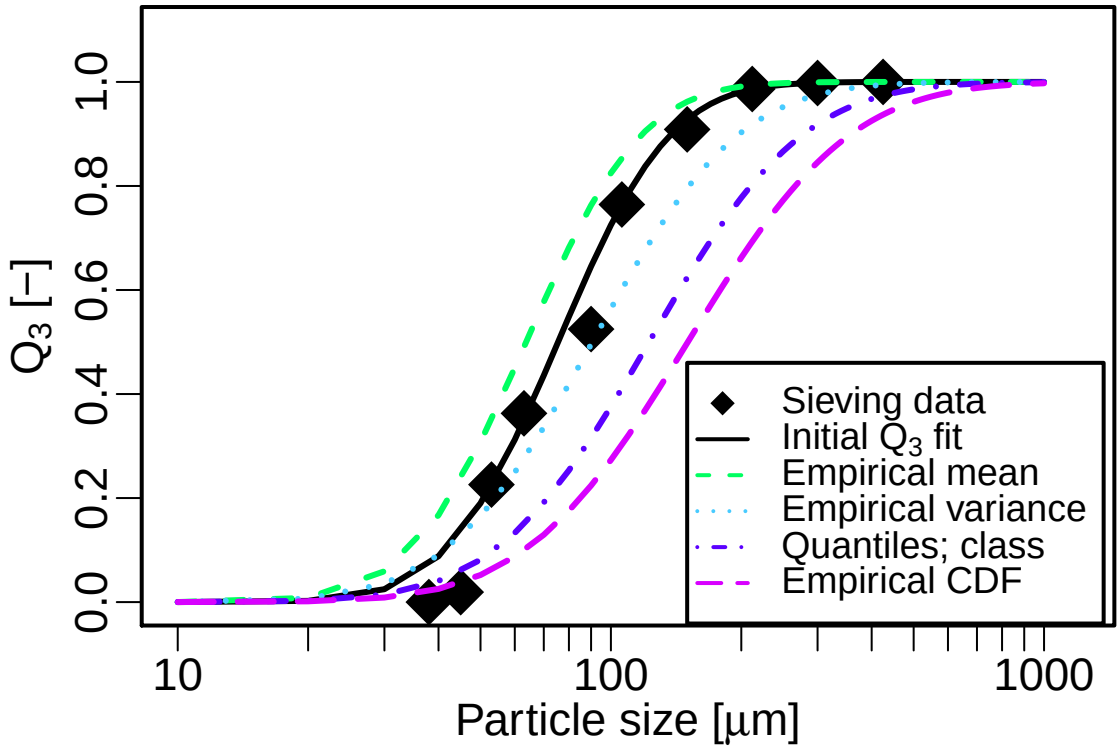

Figure 11: *Initial powder mass distribution found by various objective functions.*

respect to various characterisations of the results. Further, by using the Sobol sequences in conjunction with ranges that reflect uncertainty in the initial values, we gain insight the model and which can be related back to the physical system.

A sensitivity study performed using this method reveals two important properties with respect to the characterisation of the initial powder. First, the model input value that quantifies the height of the asperities on the particles is found to limit the model's ability to simulate simple descriptions of the particle size distribution. By allowing the parameter for the height of asperities to vary over a range when estimating the rates, the simulated particle size distribution agrees well with the experimental one when using a single value characterisation. However, the absence of experimental measurements for this value necessitates experimental investigation to ascertain if the values being selected by the optimisation process are realistic.

Second, the input parameters which describe the initial particle size distribution are found to significantly affect the distribution of the end product. When the input parameters which define the size distribution of the initial powder are allowed to vary, the model demonstrates an ability to simulate the experimental empirical size distributions. Of the two parameters which characterise the initial distribution, the shape parameter seems to be the most influential. The fact that these values are initially established by fitting a lognormal curve to sieving data suggests that this combination of methods is not appropriate for this model. Further, these observations raise questions with respect to impact that these quantities have on the experimental system.

Future work will entail experimental investigation of the properties found to be significant in this study. In particular, the effect on the end product of powders with different initial size distributions will be studied under identical process conditions. Of most interest is the shape of the initial size distribution, as the sensitivity study suggests that this is the more significant factor. Further, a detailed investigation of the initial powder will take place using a wide variety of techniques to quantify the height of asperities, such as scanning electron and atomic force microscopes, and to produce size descriptions of the initial powder by techniques more sophisticated than sieving, such as laser diffraction.

Acknowledgements

Funding by the EPSRC, grant number EP/I01165X, is gratefully acknowledged.

Nomenclature

Roman symbols

$\oslash$	Diameter	mm
d	Density function	[-]
d_i	ith element of density function	[-]
D	Cumulative mass function	[-]
D_i	ith element of cumulative mass function	[-]
e_{coag}	Coalescence coefficient of restitution	[-]
e	Particle coefficient of restitution	[-]
$e_{l_{\mathrm{i}}}$	Liquid coefficient of resistance	[-]
$e_{s_{\mathrm{o}}}$	Solid coefficient of resistance	[-]
$e_{s_{\mathrm{r}}}$	Reacted coefficient of resistance	[-]
f	Criteria function	[-]
f^{exp}	Simulation criteria	[-]
f^{sim}	Simulation criteria	[-]
h	Binder thickness	m
H_{a}	Asperities height	m
$\widehat{k}_{\mathrm{att}}$	Attrition rate parameter	sm^{-5}
$\widehat{k}_{\mathrm{coag}}$	Coalesance rate parameter	m^3
$\widehat{k}_{\mathrm{comp}}$	Compaction rate parameter	s/m
$\widehat{k}_{\mathrm{pen}}$	Penetration rate parameter	$\mathrm{kg}^{1/2}\mathrm{s}^{-3/2}\mathrm{m}^{-7/2}$
K	Coalescence collision rate	[-]
$\widetilde{K}$	Coalescence efficiency	[-]
$\widehat{k}_{\mathrm{reac}}$	Chemical reaction rate parameter	m/s
l_{e}	Volume of external liquid	m^3
l_{i}	Volume of internal liquid	m^3
m	Particle mass	kg
$\widetilde{m}$	Harmonic mass	kg
m_i	ith mass measurement	[-]
M	Number of responses	[-]
M_g	Empirical geometric mean particle size	[-]
n_{impeller}	Impeller speed	rev/s
N	Number of experimental runs	[-]
OF	Objective function	[-]
p	Pore volume	m^3
Q_0	Cumulative number distribution	[-]
q_3	Mass density distribution	[-]
Q_3	Cumulative mass distribution	[-]
R	Particle radius	m
$\widetilde{R}$	Harmonic mean particle radius	m

rpm	Revolutions per minute	[-]
s_{o}	Volume of original solid	m^3
s_{r}	Volume of reacted solid	m^3
$\mathrm{St_v}^*$	Stokes number	[-]
$\mathrm{St_v}$	Critical Stokes number	[-]
$treesize$	exponent of 2 for number of particles tracked	[-]
U_{col}	Relative particle velocity	[-]
v	Total particle volume	m^3
Var	Empirical variance	[-]
x_i	ith sieve class	[-]
x_i'	Natural log of ith sieve class	[-]

Greek symbols

$\alpha_{\mathrm{daughter}}$	Breakage; distribution	-
$\beta_{\mathrm{daughter}}$	Breakage; distribution	-
η	Binder viscosity	Pa s
μ_N	Lognormal curve location parameter; number distribution	[-]
μ_V	Lognormal curve location parameter; volume distribution	[-]
μ_{dsd}	Droplet distribution location parameter	[-]
μ_{psd}	Powder distribution location parameter	[-]
ν_{max}	Breakage; max size	-
ν_{minmax}	Breakage; proportion	-
$\rho_{l_{\mathrm{e}}}$	Binder density	$\mathrm{kg/m}^3$
$\rho_{s_{\mathrm{o}}}$	Material density	$\mathrm{kg/m}^3$
σ	Lognormal curve shape parameter	[-]
σ_{dsd}	Droplet distribution shape parameter	[-]
σ_{psd}	Powder distribution shape parameter	[-]

References

[1] T. Allen. *Particle Size Measurement*. Chapman and Hall, London, England, 4th edition, 1990.

[2] D. Ameye, E. Keleb, C. Vervaet, J. P. Remon, E. Adams, and D. Massart. Scaling-up of a lactose wet granulation process in Mi-Pro high shear mixers. *European Journal of Pharmaceutical Sciences*, 17(4–5):247–251, 2002. doi:10.1016/S0928-0987(02)00218-X.

[3] K. Ax, H. Feise, R. Sochon, M. Hounslow, and A. Salman. Influence of liquid binder dispersion on agglomeration in an intensive mixer. *Powder Technology*, 179 (3):190–194, 2008. doi:10.1016/j.powtec.2007.06.010.

[4] S. I. F. Badawy, M. M. Menning, M. A. Gorko, and D. L. Gilbert. Effect of process parameters on compressibility of granulation manufactured in a high-shear mixer. *International Journal of Pharmaceutics*, 198(1):51–61, 2000. doi:10.1016/S0378-5173(99)00445-7.

[5] S. I. F. Badawy, A. S. Narang, K. LaMarche, G. Subramanian, and S. A. Varia. Mechanistic basis for the effects of process parameters on quality attributes in high shear wet granulation. *International Journal of Pharmaceutics*, 439(1–2):324–333, 2012. doi:10.1016/j.ijpharm.2012.09.011.

[6] O. G. Batarseh, D. Nazzal, and Y. Wang. An interval-based metamodeling approach to simulate material handling in semiconductor wafer fabs. *IEEE Transactions on Semiconductor Manufacturing*, 23(4):527–537, 2010. doi:10.1109/TSM.2010.2066993.

[7] P. Bratley and B. L. Fox. Algorithm 659–implementing sobols quasirandom sequence generator. *ACM Transactions on Mathematical Software*, 14(1):88–100, 1988. doi:10.1145/42288.214372.

[8] A. Braumann and M. Kraft. Incorporating experimental uncertainties into multivariate granulation modelling. *Chemical Engineering Science*, 65(3):1088–1100, 2010. doi:10.1016/j.ces.2009.09.063.

[9] A. Braumann, M. J. Goodson, M. Kraft, and P. R. Mort. Modelling and validation of granulation with heterogeneous binder dispersion and chemical reaction. *Chemical Engineering Science*, 62(17):4717–4728, 2007. doi:10.1016/j.ces.2007.05.028.

[10] A. Braumann, M. Kraft, and P. R. Mort. Parameter estimation in a multidimensional granulation model. *Powder Technology*, 197(3):196–210, 2010. doi:10.1016/j.powtec.2009.09.014.

[11] A. Braumann, M. Kraft, and W. Wagner. Numerical study of a stochastic particle algorithm solving a multidimensional population balance model for high shear granulation. *Journal of Computational Physics*, 229(20):7672–7691, 2010. doi:10.1016/j.jcp.2010.06.021.

[12] A. Braumann, P. L. W. Man, and M. Kraft. Statistical approximation of the inverse problem in multivariate population balance modeling. *Industrial & Engineering Chemistry Research*, 49(1):428–438, 2010. doi:10.1021/ie901230u.

[13] A. Braumann, P. L. W. Man, and M. Kraft. The inverse problem in granulation modelling – two different statistical approaches. *AIChE Journal*, 57(11):3105–3121, 2011. doi:10.1002/aic.12526.

[14] C. J. Broadbent, J. Bridgwater, and D. J. Parker. The effect of fill level on powder mixer performance using a positron camera. *Chemical Engineering Journal*, 56(3): 119–125, 1995. doi:10.1016/0923-0467(94)02906-7.

[15] A. Darelius, A. Rasmuson, I. N. Björn, and S. Folestad. High shear wet granulation modelling–a mechanistic approach using populationbalances. *Powder Technology*, 160(3):209–218, 2005. doi:10.1016/j.powtec.2005.08.036.

[16] R. Dave, W. Chen, A. Mujumdar, W. Wang, and R. Pfeffer. Numerical simulation of dry particle coating processes by the discrete element method. *Advanced Powder Technology*, 14(4):449–470, 2003. doi:10.1163/156855203769710672.

[17] B. Freireich, J. Li, J. Litster, and C. Wassgren. Incorporating particle flow information from discrete element simulations in population balance models of mixer-coaters. *Chemical Engineering Science*, 66(16):3592–3604, 2011. doi:10.1016/j.ces.2011.04.015.

[18] J. A. Gantt and E. P. Gatzke. High-shear granulation modeling using a discrete element simulation approach. *Powder Technology*, 156(2–3):195–212, 2005. doi:10.1016/j.powtec.2005.04.012.

[19] J. A. Gantt, T. Palathra, and E. P. Gatzke. Analysis of the multidimensional behavior of granulation. *Journal of Materials Processing Technology*, 183(1):140–147, 2007. doi:10.1016/j.jmatprotec.2006.09.019.

[20] M. Goodson, M. Kraft, S. Forrest, and J. Bridgwater. A multi-dimensional population balance model for agglomeration. In *PARTEC 2004 - International Congress for Particle Technology*, 2004.

[21] C. R. Hicks and K. V. Turner. *Fundamental Concepts in the Design of Experiments*. Oxford University Press, New York, USA, 1999.

[22] S. M. Iveson. Limitations of one-dimensional population balance models of wet granulation processes. *Powder Technology*, 124(3):219–229, 2002. doi:10.1016/S0032-5910(02)00026-8.

[23] J. R. Jones and J. Bridgwater. A case study of particle mixing in a ploughshare mixer using Positron Emission Particle Tracking. *International Journal of Mineral Processing*, 53(1–2):29–38, 1998. doi:10.1016/S0301-7516(97)00054-9.

[24] J. R. Jones, D. J. Parker, and J. Bridgwater. Axial mixing in a ploughshare mixer. *Powder Technology*, 178(2):73–86, 2007. doi:10.1016/j.powtec.2007.04.006.

[25] P. C. Knight, T. Instone, J. M. K. Pearson, and M. J. Hounslow. An investigation into the kinetics of liquid distribution and growth in high shear mixer agglomeration. *Powder Technology*, 97(3):246–257, 1998. doi:10.1016/S0032-5910(98)00031-X.

[26] P. C. Knight, A. Johansen, H. G. Kristensen, T. Schæfer, and J. P. K. Seville. An investigation of the effects on agglomeration of changing the speed of a mechanical mixer. *Powder Technology*, 110(3):204–209, 2000. doi:10.1016/S0032-5910(99)00259-4.

[27] Z. Lin and M. B. Beck. Accounting for structural error and uncertainty in a model: An approach based on model parameters as stochastic processes. *Environmental Modelling & Software*, 27–28:97–111, 2012. doi:10.1016/j.envsoft.2011.08.015.

[28] J. D. Litster, K. P. Hapgood, J. N. Michaels, A. Sims, M. Roberts, S. K. Kameneni, and T. Hsu. Liquid distribution in wet granulation: dimensionless spray flux. *Powder Technology*, 114(1–3):32–39, 2001. doi:10.1016/S0032-5910(00)00259-X.

[29] D. W. MacFarlane, E. J. Green, and H. T. Valentine. Incorporating uncertainty into the parameters of a forest process model. *Ecological Modelling*, 134(1):27–40, 2000. doi:10.1016/S0304-3800(00)00329-X.

[30] C. Mangwandi, M. J. Adams, M. J. Hounslow, and A. D. Salman. Effect of impeller speed on mechanical and dissolution properties of high-shear granules. *Chemical Engineering Journal*, 164(2–3):305–315, 2010. doi:10.1016/j.cej.2010.05.039.

[31] B. Mishra. A review of computer simulation of tumbling mills by the discrete element method:Part I-contact mechanics. *International Journal of Mineral Processing*, 71(1–4):73–93, 2003. doi:10.1016/S0301-7516(03)00032-2.

[32] S. Mosbach, A. Braumann, P. L. W. Man, C. A. Kastner, G. P. E. Brownbridge, and M. Kraft. Iterative improvement of Bayesian parameter estimates for an engine model by means of experimental design. *Combustion and Flame*, 159(3):1303–1313, 2012. doi:10.1016/j.combustflame.2011.10.019.

[33] N. Muhammad and H. J. Eberl. Model parameter uncertainties in a dual-species biofilm competition model affect ecological output parameters much stronger than morphological ones. *Mathematical Biosciences*, 233(1):1–18, 2011. doi:10.1016/j.mbs.2011.05.006.

[34] P. Pandey, J. Tao, A. Chaudhury, R. Ramachandran, J. Z. Gao, and D. S. Bindra. A combined experimental and modeling approach to study the effects of high-shear wet granulation process parameters on granule characteristics. *Pharmaceutical Development and Technology*, 18(1):210–224, 2013. doi:10.3109/10837450.2012.700933.

[35] R. I. A. Patterson, J. Singh, M. Balthasar, M. Kraft, and J. R. Norris. The Linear Process Deferment Algorithm: A new technique for solving population balance equations. *SIAM Journal on Scientific Computing*, 28(1):303–320, 2006. doi:10.1137/040618953.

[36] J. M.-H. Poon, C. D. Immanuel, I. F. J. Doyle, and J. D. Litster. A three-dimensional population balance model of granulation with a mechanistic representation of the nucleation and aggregation phenomena. *Chemical Engineering Science*, 63(5):1315–1329, 2008. doi:10.1016/j.ces.2007.07.048.

[37] J. S. Ramaker, M. A. Jelgersma, P. Vonk, and N. W. F. Kossen. Scale-down of a high-shear pelletisation process: Flow profile and growth kinetics. *International Journal of Pharmaceutics*, 166(1):89–97, 1998. doi:10.1016/S0378-5173(98)00030-1.

[38] B. Rambali, L. Baert, and D. L. Masssart. Using experimental design to optimize the process parameters in fluidized bed granulation on a semi-full scale. *International Journal of Pharmaceutics*, 220(1–2):149–160, 2001. doi:10.1016/S0378-5173(01)00658-5.

[39] B. Rambali, L. Baert, D. Thoné, and D. Massart. Using experimental design to optimize the process parameters in fluidized bed granulation. *Drug Development and Industrial Pharmacy*, 27(1):47–55, 2001. doi:10.1081/DDC-100000127.

[40] D. Ramkrishna and A. W. Mahoney. Population balance modeling. Promise for the future. *Chemical Engineering Science*, 57(4):595–606, 2002.

[41] P. Raychowdhury. Effect of soil parameter uncertainty on seismic demand of low-rise steel buildings on dense silty sand. *Soil Dynamics and Earthquake Engineering*, 29(10):1367–1378, 2009. doi:10.1016/j.soildyn.2009.03.004.

[42] B. K. Safaie, M. Shamshirsaz, and M. Bahrami. Effect of dimensional and material property uncertainties on thermal flexure microactuator response using probabilistic methods. *Microsystem Technologies*, 16(7):1081–1090, 2010. doi:10.1007/s00542-009-0952-9.

[43] D. Suzzi, G. Toschkoff, S. Radl, D. Machold, S. D. Fraser, B. J. Glasser, and J. G. Khinast. DEM simulation of continuous tablet coating: Effects of tablet shape and fill level on inter-tablet coating variability. *Chemical Engineering Science*, 69(1): 107–121, 2012. doi:10.1016/j.ces.2011.10.009.

[44] H. S. Tan, A. D. Salman, and M. J. Hounslow. Kinetics of fluidised bed melt granulation—II: Modelling the net rate of growth. *Chemical Engineering Science*, 61(12):3930–3941, 2006. doi:10.1016/j.ces.2006.01.005.

[45] D. Verkoeijen, G. A. Pouw, G. M. H. Meesters, and B. Scarlett. Population balances for particulate processes–a volume approach. *Chemical Engineering Science*, 57 (12):2287–2303, 2002. doi:10.1016/S0009-2509(02)00118-5.

[46] D. Voinovich, B. Campisi, M. Moneghini, C. Vincenzi, and R. Phan-Tan-Luu. Screening of high shear mixer melt granulation process variables using an asymmetrical factorial design. *International Journal of Pharmaceutics*, 190(1):73–81, 1999. doi:10.1016/S0378-5173(99)00278-1.

[47] H. Zhu, Z. Zhou, R. Yang, and A. Yu. Discrete particle simulation of particulate systems: A review of major applications and findings. *Chemical Engineering Science*, 63(23):5728–5770, 2008. doi:10.1016/j.ces.2008.08.006.

[48] H. Zhu, Z. Zhou, Q. Hou, and A. Yu. Linking discrete particle simulation to continuum process modelling for granular matter: Theory and application. *Particuology*, 9(4):342–357, 2011. doi:10.1016/j.partic.2011.01.002.

[49] K. Zuurman, K. A. Riepma, G. K. Bolhuis, H. Vromans, and C. F. Lerk. The relationship between bulk density and compactibility of lactose granulations. *International Journal or Pharmaceutics*, 102(1–3):1–9, 1994. doi:10.1016/0378-5173(94)90033-7.